Colloid & Polymer Science Colloid Polym Sci 268:864–876 (1990)

Modelling the precipitation of copper oxalate aggregates

J. A. Dirksen, S. Benjelloun, and T. A. Ring

Powder Technology Laboratory (LTP), Swiss Federal Institute of Technology

Abstract: The precipitation of copper oxalate has been studied in a batch reactor. Like many other systems, the morphology of these particles suggests that they were formed by an aggregation mechanism. A mathematical model has been developed to predict particle-size distributions grown in a batch reactor, which accounts for growth by two competing mechanisms, i.e., atomistic growth and particle aggregation. The results of this model are in good agreement with experimental observations for the precipitation of copper oxalate aggregates and other spherical aggregation systems cited in the literature.

Key words: Copper oxalate; batch reactor; mathematical model; atomistic growth; particle aggregation.

Introduction

There are many chemical methods used to precipitate monodispersed spherical particles, including forced hydrolysis [1–3], controlled release of anions [4, 5] and cations [6]. Growth of monosized particles has been qualitatively described by La Mer and Dinger [7], as shown in Fig. 1. Here the concentration of the precipitating species increases with time as a chemical reaction produces an insoluble product. As the precipitate concentration continues to increase, it rises above its saturation level to a critical concentration level, at which time nucleation is induced in order to generate the needed surface area required to decrease the Gibbs free energy of the mixture. Nucleation takes place over a finite time yielding nuclei with a definite size distribution. The first nuclei produced have time to grow before the last nuclei are produced. Therefore, for shorter nucleation times the size distribution of nuclei narrows. If a monosized particle is the desired result, the shortest nucleation time possible is required. After nucleation the particles grow by atomistic growth until the supersaturation in solution decreases to zero (i.e., the equilibrium solute concentration), at which time the particles stop growing. The particles grown by atomistic growth mechanisms usually result in smooth, hard, crystalline objects with a well-defined crystal habit.

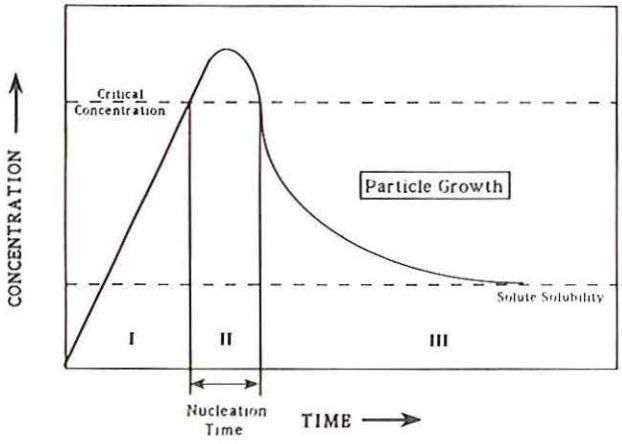

Fig. 1. Schematic representation of the nucleation and growth of monodispersed particles generated by a chemical reaction [7]

Nielsen [8] has analyzed different growth mechanism for monosized particles, including diffusion-limited, mononuclear-limited, and polynuclear-limited growth. Applying these different mechanisms, Nielsen developed chronomal analysis, which accounts for the increase in particle size as a function of time. Experimental results [9–11] have shown that Nielsen's chronomal analysis does indeed account for the change in particle-size with time, but the

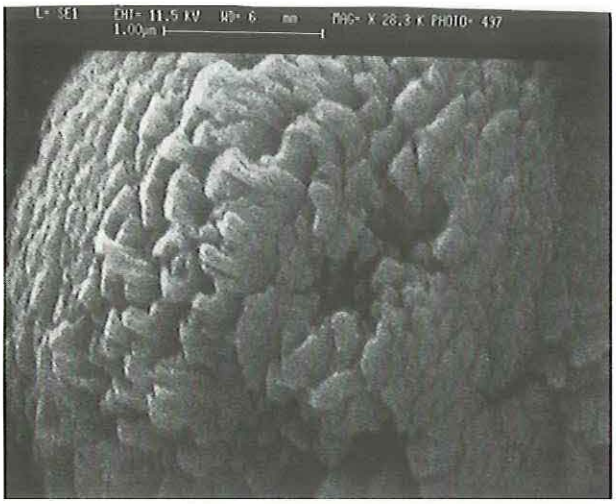

Fig. 2. Typical SEM photograph of a single copper oxalate sphere showing the submicron growth units that make-up the aggregate particle. This sphere was prepared using reactant concentrations of 0.134 M $Cu(NO_3)_2$/0.263 M $H_2C_2O_4$. The final sample was removed after aging for three days

diffusion coefficients obtained from this analysis are several orders of magnitude smaller than molecular diffusion or unit-cell diffusion in liquids. This result suggests that this analysis is in error.

Overbeek [12] has reviewed various growth models and discussed the ramifications each growth mechanism has on the relative standard deviation of a particle-size distribution. He has found that for reaction-limited growth, the particle-size distribution broadens as the particles grow; with surface-nucleation-limited growth the breadth of the particle-size distribution remains constant as the particles grow and for diffusion-limited growth the particle-size distribution narrows with time.

This paper studies the precipitation of hydrous copper oxalate from solution as a test case. The morphology of the copper oxalate produced suggests that the particles are formed by an aggregation process as illustrated by the scanning electron micrograph (SEM) in Fig. 2. This type of particle morphology is often observed in the literature, dating back to the work of Tezak et al. [13–15] from the 1960s to the present [4, 6, 16, 17]. For this reason, a new mathematical model has been developed. It accounts for nucleation and particle growth by two competing mechanisms: atomistic growth and particle aggregation. Particle aggregation is considered by applying an adaptation of Smoluchowski's rapid flocculation theory [18]. This new theory is applied to the experimental results for generating copper oxalate aggregates as well as other spherical aggregates extracted from the literature.

Experimental Methods

Materials

The reactant solutions were prepared using de-mineralized water as the solvent for the two reactant preparations. The oxalic acid ($H_2C_2O_4$) was obtained from Fluka Chemical (Buch, Switzerland) and the $Cu(NO_3)_2 \cdot 3H_2O$ from Merck (Zurich, Switzerland). The colloidal suspension produced from the precipitation was stabilized using reagent grade (99.9 %) absolute ethanol doped with 0.1 % (by weight) hydroxypropylcellulose (HPC, MW 30 000–50 000), as supplied by Nippon Soda Company, Tokyo, Japan. These raw materials were used as purchased without any further modifications.

Methods

The precipitation of copper oxalate aggregates was accomplished at 20 °C by the following reaction:

$$Cu(NO_3)_2 + H_2C_2O_4 <=> CuC_2O_4 + 2HNO_3.$$

Two 250 ml solutions – one of 0.55 M $Cu(NO_3)_2$ and the other of 1.1 M $H_2C_2O_4$ – were added to a baffled (500 ml) batch reactor. These two solutions were added to the reactor within 15 seconds. The mixing rate in this reactor during these experiments was held constant at 500 rpm, which was sufficient to maintain a uniform slurry. Samples were extracted from the midpoint of the reactor using a 5 ml pipette at various sample times throughout the experiment. Samples were taken at 1, 5, 10, 30, 60, 120, and 180 minutes after nucleation. The extracted sample was immediately added to a 50 ml ethanol / (HPC) solution to stop further aggregation. Reaction density (i.e., the precipitated CuC_2O_4 concentration) was also measured throughout this study by extracting 50 ml of reaction slurry with a 50 ml pipette and filtering the mixture using 0.2 μm filter paper. Copper oxalate cake was dried for 8 hours at 50 °C and then weighed. Slurry density was found to be 44.805 ± 0.033 mg CuC_2O_4/ml of reaction mixture for all samples times, which gives a reaction yield of 100 %. Particle size distributions were measured on each time-dependent sample using a Horiba CAPA-700 Disc Centrifuge (Kyoto, Japan). Range of detection for this particular study was set to be sensitive to particle sizes within the range of 0.1–3.0 μm. Density measurements were performed on the copper oxalate product using a Helium Pychnometer (Micromeritics, Norcross, Georgia, USA). The density of the dried copper oxalate particles was found to be 3.5 ± 0.125 g/ml.

Experimental results

Figure 3a–d shows transmission electron micrographs (TEM) of the copper oxalate particles produced at various times after nucleation. One minute after reactant introduction, a plethora of particles on the order of ~ 0.01 μm in diameter are prevalent. At

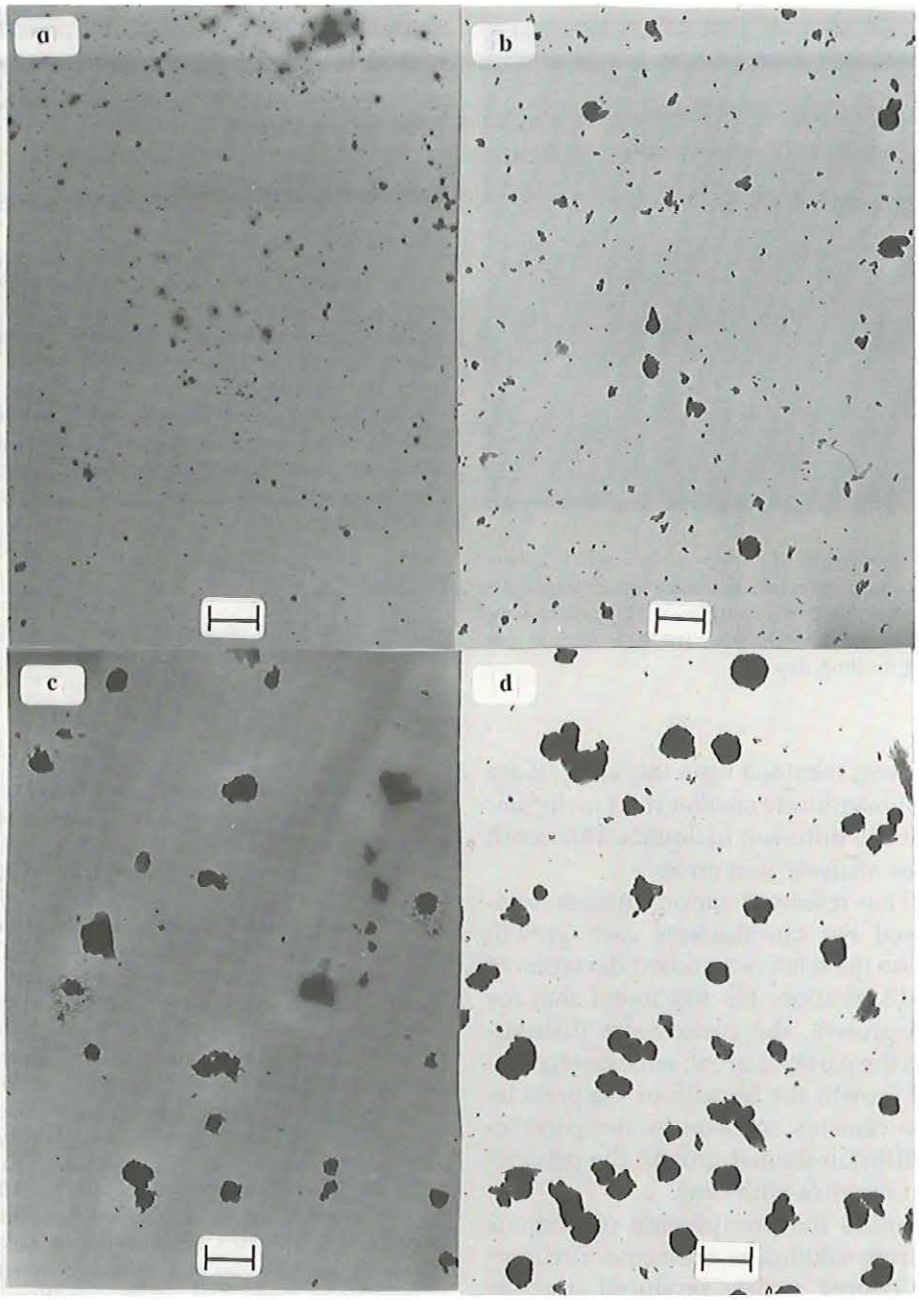

Fig. 3 (a-d). TEM photographs of copper oxalate product prepared using reactant concentrations of 0.55 M $Cu(NO_3)_2$ / 1.1 M $H_2C_2O_4$. Sequence shows the particles produced at different times, where: a) 1 min, b) 10 min, c) 60 min, d) 120 min after nucleation. Bar = 0.60 μm

the same time, a small fraction of the particles are present as aggregates 0.1 μm in diameter. As the time after nucleation increases, the number density of 0.01 μm particles decreases and their size increases slightly. Size of the aggregate particles also increases as time increases until they reach their steady state size of o.27 μm, three hours after mixing. At this time, the number density of ~ 0.01 μm particles has nearly disappeared. The aggregate structure, which results 30 minutes after reactant introduction, is clearly shown in the higher magnification TEM in Fig. 4.

Particle size distributions of aggregate particles

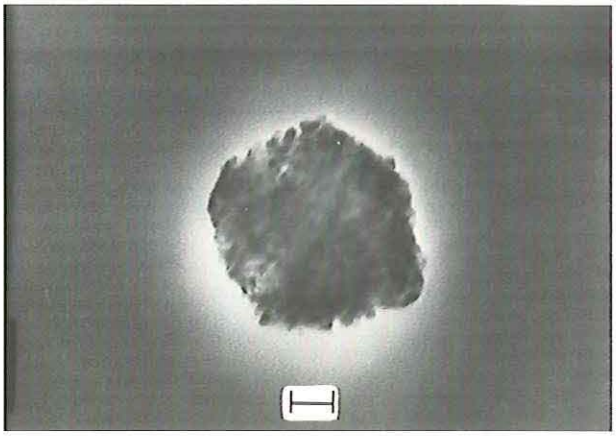

Fig. 4. Higher magnification TEM of a copper oxalate sphere showing the very small growth units comprising a particle, corresponding to conditions in Fig. 3d. Bar = 0.04 μm

larger than 0.1 μm were measured by the Horiba disc centrifuge. The measured distributions are shown in Fig. 5 for several aging times. The main population of aggregates after 1 min is below the lower limit of detection of the instrument. After 5 min, the population of 0.01–0.2 μm particles increases, indicating that additional aggregates were still growing into a size range where the particles could just be detected by the disc centrifuge. As time progressed further, the size of the aggregates increased and the width of the size distribution decreased, as shown in Fig. 5. A plot of the median size and the relative standard deviation of the aggregate size distribution as a function of time is given in Figs. 6 and 7, respectively.

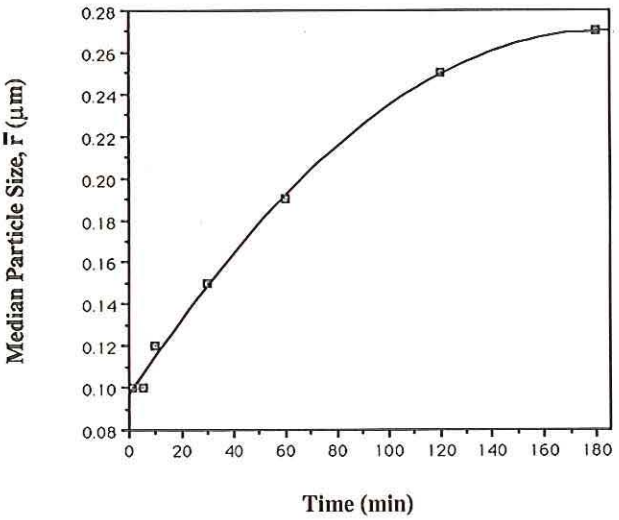

Fig. 6. Median size of copper oxalate spheres as a function of aging time

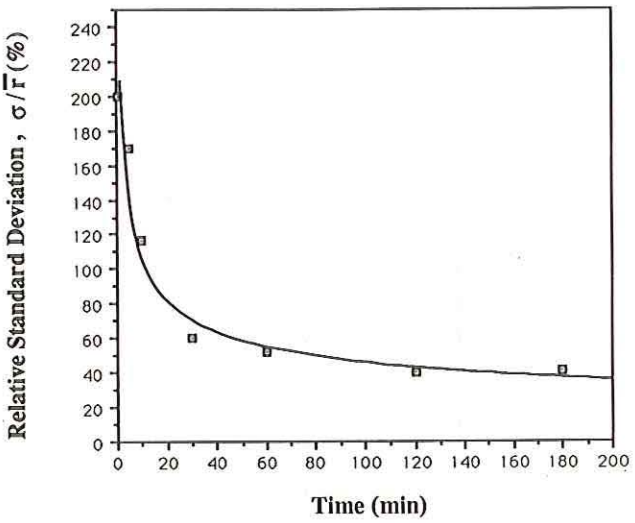

Fig. 7. Relative standard deviation of copper oxalate spheres as a function of aging time

Median size increased from 0.1 μm to 0.27 μm during the 3 h of this experiment. Relative standard deviation decreased from 200 % to 40 % during the same time.

Discussion

Decrease in the relative standard deviation with aging time – as described by Overbeek [12] – suggests that the rate-determining step for particular growth is the diffusion of the growth units through a boundary layer surrounding the particles. In an attempt to further distinguish between the particle growth mechanisms, chronomal analysis [8] was also used. This anaylsis has been comprehensively described by Nielsen and may be applied to systems that consist of particles of uniform size and shape and have a constant number density of particles. Chronomal analysis is especially useful for systems that generate an insoluble species and where the concentration of molecular precipitate changes with time.

Based on chronomal analysis, a linear plot of the diffusion chronomal I_d [a function of the size of the particle $r(t)$] given by:

$$I_d = \frac{1}{2}\ln\left[\frac{(1-\alpha_d)}{(1-\alpha_d^{1/3})^3}\right] - \sqrt{3}\tan^{-1}\left[\frac{\sqrt{3}}{1+2\alpha_d^{1/3}}\right]$$

with

$$\alpha_d = [r(t)/r_\infty]^3 ,$$

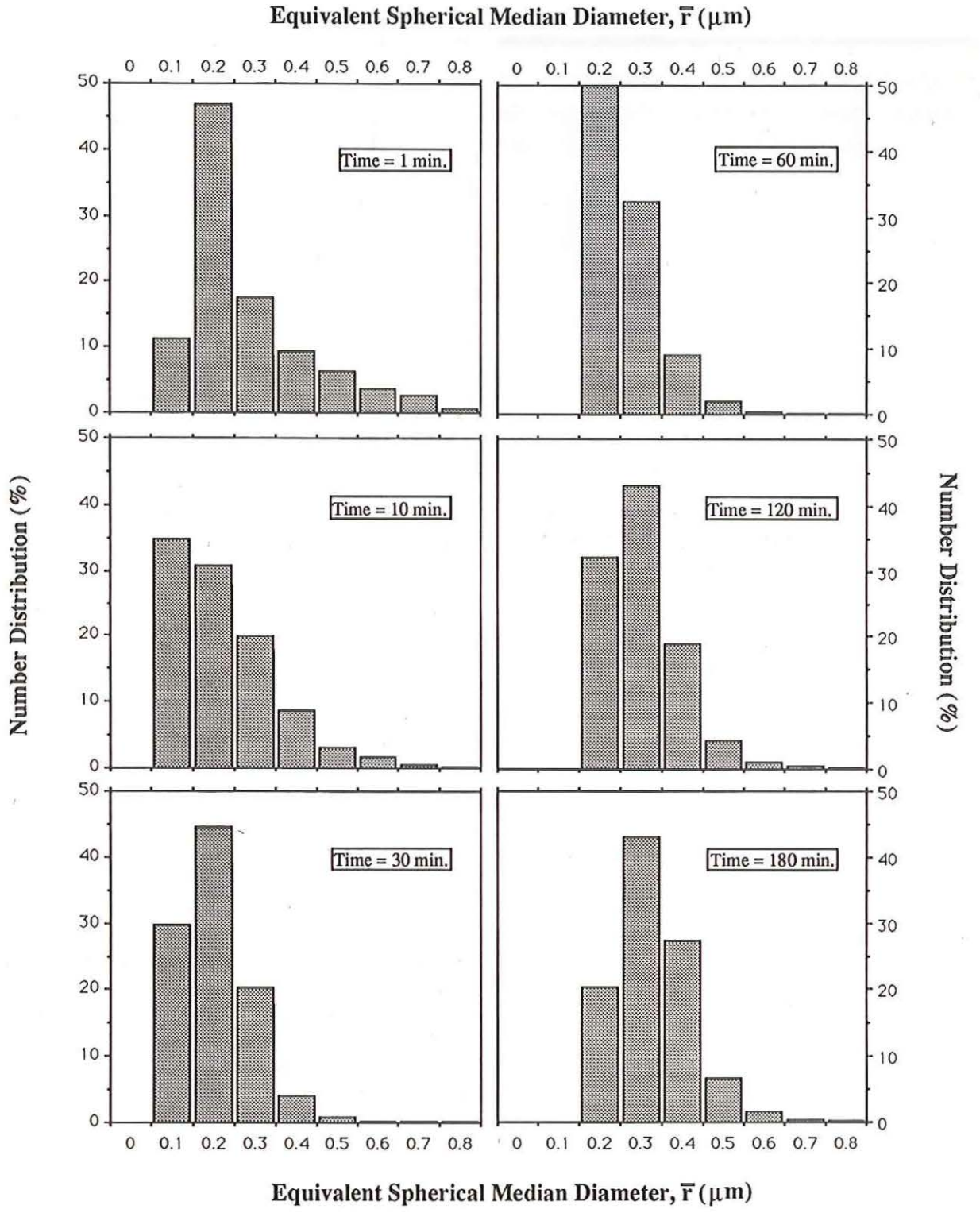

Fig. 5. Number distribution for copper oxalate particles measured with disc centrifuge at various times

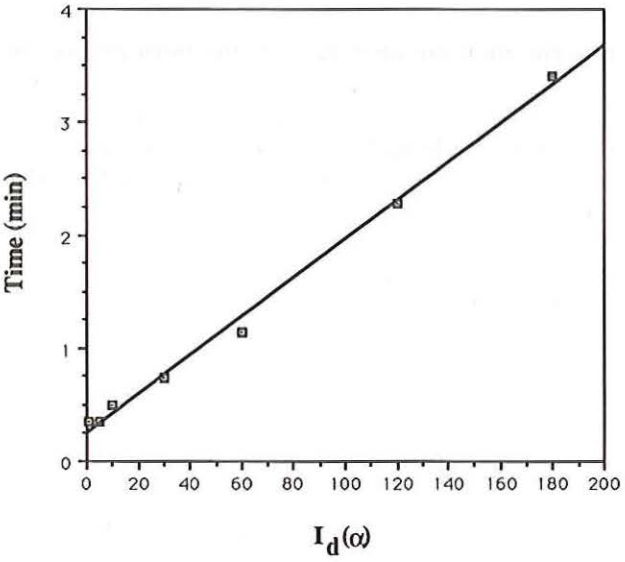

Fig. 8. Chronomal analysis applied to copper oxalate data for diffusion-controlled growth

versus time exists if diffusion is the rate-limiting step of particle growth. The slope of this line, K_d (= $r_\infty^2/(3vD[C^\circ - C_\infty])$, is inversely proportional to the molecular diffusion coefficient, D. A plot of this linear relationship is shown in Fig. 8 for copper oxalate growth, and has a correlation coefficient (r^2) of 0.972. Chronomal analysis was also performed for polynuclear growth with a degree of reaction ranging from 2 to 4. In each case, the plots were non-linear (i.e., $r^2 < 0.9$), suggesting that the rate-limiting step during particle growth was not by a polynuclear mechanism. The linear diffusion chronomal plot, along with the decrease in the relative standard deviation, suggests that diffusion in solution is the rate-limiting step during copper oxalate particle growth. Diffusion coefficients obtained from chronomal analysis for the copper oxalate study as well as for other typical monodispersed systems, namely that of Jean and Ring [9] and Ogihara et al. [10], are listed in Table 1. These diffusion coefficients are several orders of magnitude smaller than molecular diffusion in liquids (i.e., ~ 10^{-5}/s). Also listed in Table 1 are the diameters of the diffusing species as calculated from the diffusion coefficents using the Stokes-Einstein equation [19]. These calculated diameters are larger than the measured particle sizes by factors ranging from 5–2 500, suggesting that either molecular diffusion is not the rate-limiting step or this analysis is in error.

In order to quantify a kinetic expression for the rate-limiting step in particulate growth and justify the aggregate morphology of the precipitated particles, as shown in Fig. 2, a new model for the precipitation of monosized particles has been developed. This model accounts for the nucleation, atomistic growth, and aggregation in the formation of particles.

Table 1. Diffusion coefficients from chronomal analysis and calculated size of diffusing species from Stokes-Einstein's relationship

System	Diffusion coefficient (cm^2/sec.)	Stokes-Einstein Size (μm)
Copper oxalate	2.83×10^{-12}	759
Zirconia [10]	3.91×10^{-10}	7.6
Titania[9]	1.14×10^{-9}	1.5

Model development

Macroscopic population balance

Particulate growth, and consequently particle size distributions, can be modelled by applying a macroscopic population balance, as described by Randolph and Larson [20]. The functional form of this population balance for a well-mixed, constant volume batch reaction can be written as follows:

$$\frac{\partial \eta(L,t)}{\partial t} + G\frac{\partial \eta(L,t)}{\partial L} = B(L,t) - D(L,t). \quad (1)$$

(See the nomenclature section at the end of this paper for the definitions of the symbols used.) The first term in this partial differential equation describes the population's time rate of change, η; the second term describes the atomistic growth of the particles (which assumes that G is independent of particle size L); and finally the last two terms account for the birth and death of particles of size L and aggregation mechanism. The birth function describes the rate at which particles enter a particle size range L to $L+\Delta L$, and the death function describes the rate at which the particles leave this control volume. Randolph and Larson do not include the birth and death terms in their analysis, consequently ignoring particulate growth by aggregation mechanisms and only concentrating on atomistic growth. This population balance also assumes a negligible volume accumulation due to particle breakage.

Considering the La Mer concept [7] for the precipitation of particles shown in Fig. 1, an initial con-

dition for the population balance corresponding to an initial burst of nuclei can be given by

$$\eta(L,t=0) = \eta^1 (L_0, t=0), \tag{2}$$

where the population of nuclei η^1 either decreases with time due to aggregation and atomistic growth of the nuclei out of size L_0, or increases with time due to further nucleation. Atomistic growth is accounted for in the second term of Eq. (1). In this work, we will only consider a single burst of nuclei generated at time zero ($\eta^0(L_0, t=0) = \eta^0 =$ constant). Aggregation of these nuclei gives the following time dependence with respect to the nuclei population, as described by Smoluchowski [18] and Ives [21]

$$\eta^1(L_0,t) = \frac{\eta^0}{(1+t/t_{1/2})^2}, \tag{3}$$

where $t_{1/2} = (1/K\eta^0 L_0)$ is the aggregation half life. The reader should be reminded that the nuclei – as with all other particle sizes in the distribution – can grow into and out of a size range by atomistic growth and/or particle aggregation. Thus, the population balance, as described in Eq. (1), is useful in that it predicts the number distribution of particles grown under kinetically competing conditions: that of atomistic growth and particle aggregation. For a solution to the population balance to be possible, mathematical relationships must be developed for the birth and death functions accounting for particle aggregation.

Rapid flocculation theory

The birth and death functions predict the importance of particulate aggregation on the final particle-size distribution. The key concepts for the development of these two functions come from Smoluchowski's rapid flocculation theory [18], which predicts the rate of change in a population density of an aggregate of k particles:

$$\frac{\partial N_k}{\partial t} = \frac{1}{2}\sum_{i=1}^{i=k-1}\sum_{j=k-i}^{j=k-1} 4\pi R_{ij} D_{ij} N_i N_j$$

$$- N_k \sum_{i=1}^{\infty} 4\pi R_{ik} D_{ik} N_i. \tag{4}$$

The two summation terms on the right-hand side of this equation are analogous to the birth and death functions, respectively. Changing the form of this equation to fit the form of the population balance equation – while at the same time making the appropriate substitutions for the terms R_{ij} and D_{ij} – the birth and death functions can be written as follows:

$$B(L,t) - D(L,t) = \frac{1}{r_k}\frac{\partial N_k}{\partial t}$$

$$= \frac{k_B T}{3\mu r_k}\sum_{i=1}^{i=k-1}\sum_{j=k-i}^{j=k-1}\frac{(r_i+r_j)^2}{r_i r_j} N_i N_j$$

$$- \frac{2k_B T}{3\mu r_k} N_k \sum_{i=1}^{\infty}\frac{(r_i+r_k)^2}{r_i r_k} N_i. \tag{5}$$

The birth and death functions are now on a per particle size basis, the same as used in Eq. (1). Some key substitutions become necessary to further simplify these functions:

$$N_T = \int_0^{\infty} \eta(x)dx$$

$$\begin{aligned} N_i &= x\eta(x) & r_i &= x \\ N_j &= (L-x)\eta(L-x) & r_j &= (L-x) \\ N_k &= L\eta(L) & r_k &= L \end{aligned} \tag{6}$$

$$\sum_{i=1}^{i=k-1}\sum_{j=k-i}^{j=k-1} N_i N_j = \frac{1}{L}\int_0^L \eta(x)\eta(L-x)dx \qquad \sum_{i=1}^{\infty} N_i = \frac{1}{L}\int_0^{\infty}\eta(x)dx.$$

Substitution of these relationships into Eq. (5) yields

$$B(L) = K\int_0^L \eta(x)\eta(L-x)\,dx \tag{7}$$

$$D(L) = 2K\eta(L)\frac{1}{L^2}\int_0^{\infty}(x+L)^2\eta(x)dx$$

$$= 2K\eta(L)N_T\left[\frac{\overline{(x^2)}}{L^2} + \frac{2\bar{x}}{L} + 1\right], \tag{8}$$

where the aggregation-rate constant is

$$K = \frac{k_b T}{3\mu W} \tag{9}$$

and W is the average colloid stability factor for the system. A colloid stability factor of one corresponds to the case where the particles stick together every time they collide (i.e., a very unstable system). This case corresponds to a sticking probability of one and is proportional to the particles' rate of birth and death. The $i^{\underline{th}}$ moment is described as

$$\overline{(x^i)} = \frac{\int_0^\infty x^i \eta(x)dx}{\int_0^\infty \eta(x)dx} = \frac{\int_0^\infty x^i \eta(x)dx}{N_T}. \tag{10}$$

Applying the new birth and death functions given in Eq. (7) and (8), respectively, the governing differential equation for the population of particles $\eta(L,t)$ becomes

$$\frac{\partial \eta(L,t)}{\partial t} + G\frac{\partial \eta(L,t)}{\partial L} = K\int_0^L \eta(x)\eta(L-x)dx$$

$$-2K\eta(L)N_T\left[\frac{\overline{(x^2)}}{L^2} + \frac{2\bar{x}}{L} + 1\right]. \tag{11}$$

An analytical solution to this integro-differential equation is impossible without simplifying assumptions. The birth function can be simplified by assuming that aggregation takes place by the collision of nuclei with the larger aggregates and not by the collision of particles of similar sizes, either nuclei-nuclei or aggregate-aggregate. By limiting the type of growth mechanism by which a particle can be born, the convolution integral describing the birth function can be solved as

$$B(L) = K\eta^1 L\eta(L). \tag{12}$$

Certainly, this assumption is not valid for all times. However, for much of the time after the initial burst of nucleation, this is probably the case for the following two reasons: first, because there is a high number density of nuclei compared to the aggregates, the probability of a collision between a large aggregate particle and a nuclei is higher than the collision between two larger aggregates. Second, the colloid stability factor W is different for each type of collision. The sticking probability (α $1/W$) for a collision between two nuclei or two aggregates is low while the sticking probability for the collision between a nuclei and an aggregate is much higher – approaching 1.0.

With this simplifying assumption in mind [i.e., Eq. (12)], the new population balance becomes

$$\frac{\partial \eta(L,t)}{\partial t} + G\frac{\partial \eta(L,t)}{\partial L} = K\eta^1 L\eta(L)$$

$$-2K\eta(L)N_T\left[\frac{\overline{(x^2)}}{L^2} + \frac{2\bar{x}}{L} + 1\right]. \tag{13}$$

This partial differential equation can be approximated by an ordinary one by creating a new characteristic variable, i.e., $\tau = L/G - t$. Applying the initial condition for this problem, the characteristic can be shown to be a constant, i.e., $\tau = L_0/G$. Making this variable transformation, the new characteristic population balance becomes

$$2G\left[\frac{\partial \eta(L,t)}{dL}\right]_\tau = K\eta^1 L\eta(L)$$

$$-2K\eta(L)N_T\left[\frac{\overline{(x^2)}}{L^2} + \frac{2\bar{x}}{L} + 1\right]. \tag{14}$$

By applying this transformation under conditions of constant τ, the dimensionless solution to the characteristic population balance for a batch reactor can be found to be

$$\frac{\eta(L)}{\eta^1} = \mathrm{EXP}\left\{-\beta\left[\left(L/L_0 - 1\right) - \frac{\Phi}{4}\left(\left(L/L_0\right)^2 - 1\right.\right.\right.$$

$$\left.\left.\left. + \frac{\overline{(x^2)}}{L_0^2}\left(1 - \left(L_0/L\right)\right) + 2\frac{\bar{x}}{L_0}\ln\left(L/L_0\right)\right]\right\}, \tag{15}$$

where

$$\beta = \frac{KN_T L_0}{G} \quad ; \quad \Phi = \frac{\eta^1 L_0}{N_T}. \tag{16}$$

The dimensionless group β corresponds to the ratio of the aggregation rate to the rate of atomistic growth.

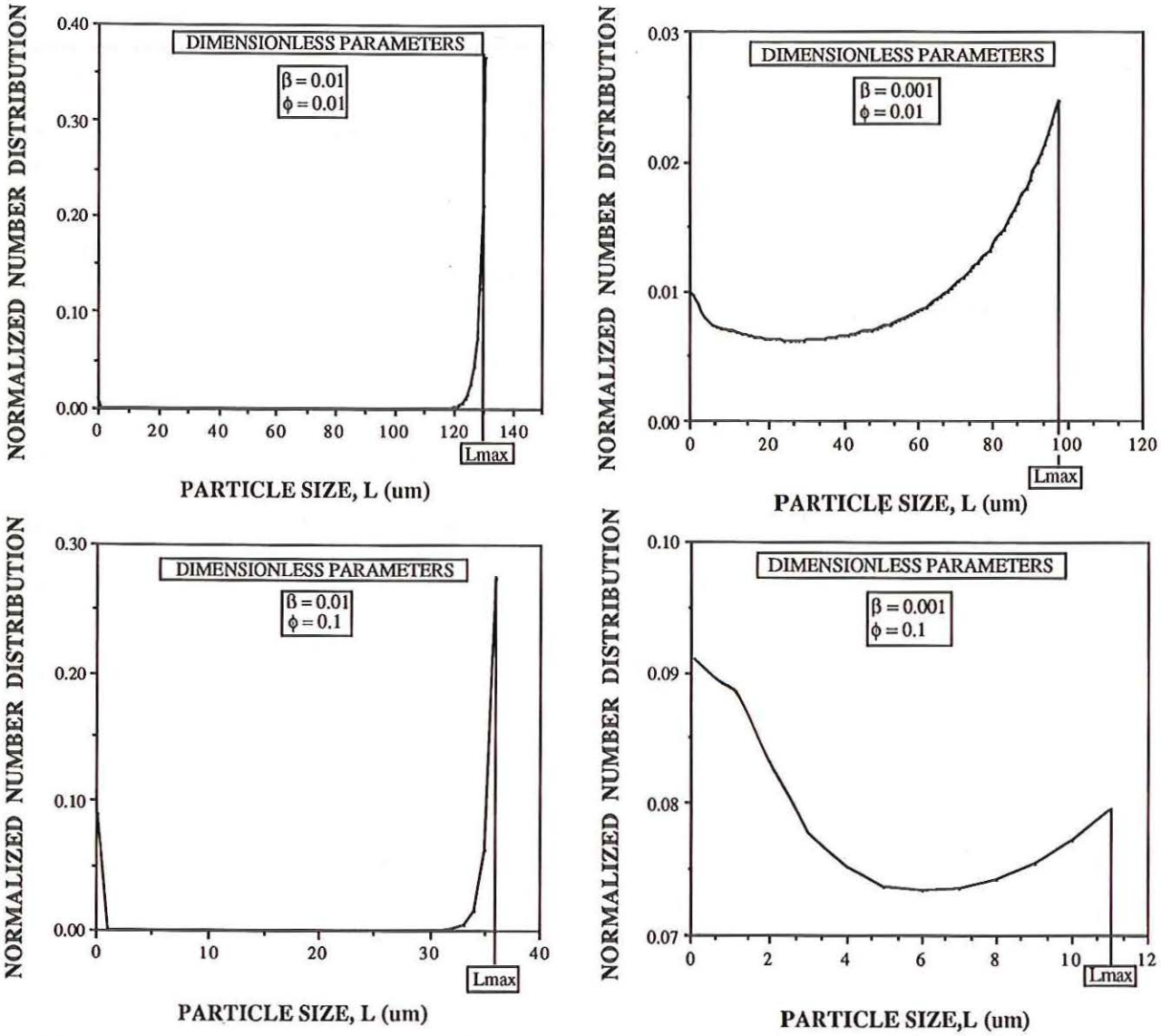

Fig. 9. Theoretical prediction of particle size distributions in a batch reactor for a) $\phi = 0.01$ and $\beta = 0.01$, b) $\phi = 0.01$ and $\beta = 0.001$, c) $\phi = 0.1$ and $\beta = 0.01$, and d) $\phi = 0.1$ and $\beta = 0.001$. The values of the constants used for these calculations are $K = 1.37 \times 10^{-15}$ l/sec, $L_0 = 0.1$ μm, $x = 3.76$ μm, $x^2 = 22.7$ μm, T = 363 K, $\mu = 0.31$ cp, $N_T = 5.6 \times 10^{11}$ No./1, and $\eta^1 = 8 \times 10^{11}$ No./1 μm

Large values of β suggest that aggregation is fast compared to atomistic growth, while small values of β suggest that atomistic growth dominates. The dimensionless number Φ corresponds to the fraction of the toal number of particles that are nuclei. Both β and Φ are negative functions of time; that is to say, as the time increases both of these dimensionless groups decrease.

Recall that this solution to the population balance is only valid under conditions of constant τ, which means that for every particle of size L there is a corresponding time needed for its formation.

A physical constraint on the population balance

A physical constraint must be placed upon the population balance to ensure that the conservation of mass is upheld. Mathematically, this means that the following population balance relationship must hold:

$$N_T(t) = \int_{L_0}^{L_{max}} \eta(x,t)dx. \tag{17}$$

The maximum particle size present, L_{max}, is the constraint in this population balance. This means that for fixed values of B, Φ, and time, the final distribution – including the maximum particle size – can be predicted.

The qualitative effect of β and Φ on the particle size distribution is shown in Fig. 9. When β and Φ are equal to 0.01 (Fig. 9a), we find a bimodal size distribution consisting of a small population of nuclei and a narrow size distribution of aggregates with nothing in between the two modes. This plot is characteristic of the final stages of aggregation. When Φ is increased to 0.1 and β remains the same (Fig. 9b), we find a larger population of nuclei. The aggregate size is smaller and the relative standard deviation of the aggregates is larger than in Fig. 9a. Figure 9b is also characteristic of the final stages of aggregation, but earlier in time than the example in Fig. 9a. When β is 0.001 and Φ is 0.01 (Fig. 9c), we find a broad and continuous distribution of particle sizes between the nuclei and the maximum sized aggregates. Increasing the value of Φ to 0.1 (Fig. 9d), we find that the maximum size is decreased drastically and the shape of the size distribution is changed by putting more emphasis on the population of nuclei than on the aggregate population, which is typical of an earlier snapshot in time – corresponding to an increase in Φ.

Comparison of model with experiment

This new model predicts that a bimodal particle size distribution can be formed during nucleation, growth and aggregation under certain conditions. One of the modes will be made up of nuclei – of a size predicted by homogeneous nucleation theory – and the other mode will be made up of aggregates. This bimodal size distribution is clearly evident in the TEM pictures (for our example copper oxalate), shown in Fig. 3. Employing image analysis for counting and sizing the particles shown in Fig. 3 is difficult to do accurately because the two main sizes of particles are different by a factor of 100 to 1 000. For this reason, quantitative validation of the theoretical particle size distribution with the experimental size distribution cannot be made at this time. However, a quantitative comparison of the growth kinetics of the aggregates can be made between experiment and theory.

From the characteristic time τ (and its value due to the initial condition), the increase in nuclei size with time is defined as

$$L = L_0 + Gt \tag{18}$$

for a constant atomistic growth rate G. Equation (18) can be written in its differential form as

$$dL/dt = G. \tag{19}$$

Because of our limitations in the particle-size analysis for the nuclei, we must transform this rate expression into one we can measure. This transformation can be made by noting that the initial aggregate of size λ_0 is composed of m nucleii of size L_0, givig a conservation equation

$$\lambda_0^n = mL_0^n, \tag{20}$$

where n is the fractal dimension [22] of the aggregate. Therefore, for a fractal dimension of 1 (i.e., $n = 1$) a linear aggregate results, and for $n = 3$ a spherical aggregate results. By multiplying Eq. 19 by the dimensionless group β [as defined in Eq. (16)] and making the definition that the aggregate growth rate $d\lambda/dt \equiv KN_T\lambda^0$, we can now state a new rate expression for the aggregate growth rate $d\lambda/dt$ as

$$\frac{d\lambda}{dt} = \lambda_0 KN_T = \sqrt[n]{m}\, L_0 KN_T, \tag{21}$$

where N_T is the total number of particles per unit volume, which is also a function of time given by [20]

$$N_T = \frac{N_0}{(1 + t/t_{1/2})}. \tag{22}$$

Integrating Eq. (20) with the appropriate substitution yields

$$\lambda - \lambda_0 = \lambda_0 \ln (1 + t/t_{1/2}) = \sqrt[n]{m}\, L_0 \ln (1 + t/t_{1/2}). \tag{23}$$

This simple expression describes the change in the aggregate size λ as a function of time. The experimental data shown in Fig. 6 are replotted in the form of the above expression as illustrated in Fig. 10. A linear regression of the copper oxalate data shows a correlation coefficient (r^2) of 0.995 when the half life $t_{1/2}$ was 43 min. The value of $t_{1/2}$ used gave the

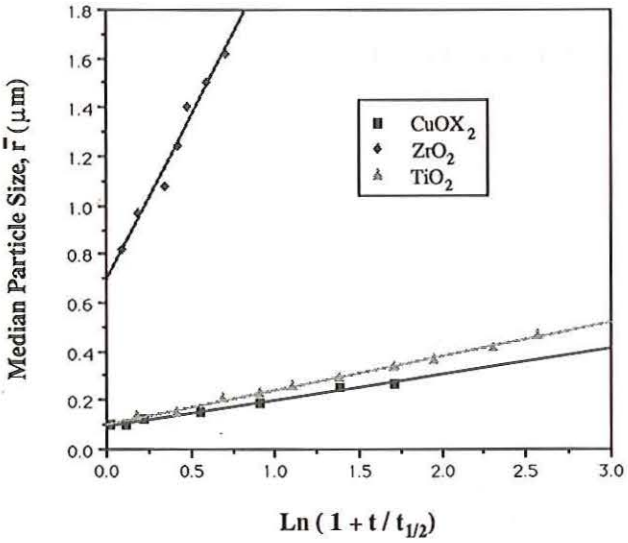

Fig. 10. Characteristic analysis from the new spherical aggregation model. Where the copper oxalate is prepared as described above, and the ZrO_2[10] and the TiO_2[9] are prepared using alkoxide routes

maximum correlation coefficient (r^2) in the linear regression. A minimization of the sum-of-squares technique is needed to perform this iteration. Performing a non-linear regression on the data with the proposed model using a three-parameter fit [i.e., λ_0 (slope), λ_0 (intercept) and $t_{1/2}$] also can be accomplished with the same results. If $t_{1/2}$ is known from colloid stability information, then a simple linear regression may be preformed. Other data from Jean and Ring [9] and Ogihara et al. [10] are also plotted in Fig. 10, showing similar linearity and similar correlation coefficients. The resulting coefficients obtained from the slopes and intercepts and "optimum" aggregation half life $t_{1/2}$, obtained from Fig. 10 are given in Table 2. The value of λ_0 (intercept) is reasonable compared to the initial aggregate size observed in the TEM photos shown in Fig. 3a.

Equation (23) proposes that aggregation controlled growth is the rate limiting step; therefore, if the model fits the data and the constraints of its development are met, then one can conclude that the rate-limiting step in a particular reaction is aggregation controlled growth. This constraint can be proved or disproved by setting up the null hypothesis H_0 where

$$H_0 : \lambda_0 \text{ (slope)} = \lambda_0 \text{ (intercept)}$$

$$H_a : \lambda_0 \text{ (slope)} \neq \lambda_0 \text{ (intercept)}$$

Recall that this statistical analysis will only tell us if the reaction is purely aggregation controlled. Therefore, for systems that change growth mechanisms, the null hypothesis will be rejected within some level of confidence. This analysis has been completed for the systems of interest in this paper. Table 2 compiles these results showing whether the null hypothesis has been accepted or rejected for each particular system based upon a 95 % confidence level. Therefore, the only true diffusion controlled growth mechanism of the three studied, is the copper oxalate system.

Table 2. Results from characteristic analysis

System	λ_0 (slope) (μm)	λ_0 (intercept) (μm)	$t_{1/2}$ (min)
Copper oxylate	0.109	0.097	43
Zirconia[10]	1.334	0.692	291
Titania[9]	0.146	0.109	12

* The null hypothesis states that the reaction is diffusion controlled at a 9 5% confidence level

Constraints placed on this model make it much harder to accept the diffusion-limited case than the previously studied chronomal analysis. Unlike the chronomal analysis, this theory will only describe the particle growth by one mechanism. This means that for examples like Titania and Zirconia, it is not so surprising that we cannot confidently say that the growth of these particles is solely by an aggregation-limited process. It is a common belief that particle growth may not follow just one mechanism throughout the whole process. It is quite possible to think that Titania may grow under polynuclear conditions in the early stages of growth and switch to aggregation-limited conditions at some later point. However, under these conditions the model for aggregation-limited growth will not be able to predict the size of particles over the entire precipitation process (i.e., rejection of the null hypothesis). The difference between the three reactions studied is the varying levels of supersaturation for each reaction mixture. The highest being the copper oxalate system and the lowest level of supersaturation being the Zirconia system. With the highest supersaturation, nucleation dominates atomistic growth, and this aggregation model is expected to fit the data reasonably well. But at low supersaturations, nucleation and growth are similar, and this simple theory (Eq. 23) is not likely to fit the data as well.

Conclusions

Like many examples in the literature, the precipitation of spherical copper oxalate particles gives an aggregate particle morphology. The growth rate of copper oxalate aggregates was studied using TEM and particle size analysis using a disc centrifuge. These results fit the Nielsen chronomal analysis, but give a diffusion coefficient that is several orders of magnitude smaller than for molecular diffusion coefficients. As a result of these low diffusion coefficients and the non-crystalline aggregate structure of the precipitated particles, a mathematical model has been developed to help predict particle-size distributions in a batch reactor. This model accounts for nucleation, atomistic growth, and aggregation. An analytical solution to this model was found by applying the following simplifying assumptions:

1. The most frequent collisions for growing aggregates are those of the largest particles with the smallest particles.
2. The rate of atomistic growth is independent of particle size.
3. Particle breakage is negligible.

This model predicts that the aggregates increase in size with a natural logarithm dependence on time. For the copper oxalate and several other systems, this behavior is observed. This model also predicts a bimodal size distribution, one mode of nuclei which grow atomistically, and the other mode of aggregates which grow by aggregation. These bimodal particle-size distributions are observed in the TEM pictures taken of the precipitating particles, and has been seen for many years in various precipitation processes.

Acknowledgement

The authors would like to acknowledge the fruitful discussions of Dr. Paul Bowen and Dr. Dennis Gallager. TEM analysis was performed by Dr. Tiziana Stoto and SEM analysis was performed by Silvia Ampero and Dr. Dennis Gallager. This research was sponsored by the Swiss National Science Fund, National Program 19.

Nomenclature

$B(L)$	Birth function on a per particle basis **No./L^3.L.Θ.**
$D(L)$	Death function on a per particle basis **No./L^3.L.Θ.**
D_{ij}	Effective diffusivity of i^{th} and j^{th} particles **L^2/Θ**
G	Growth rate **L/Θ.**
H_a	Alternative null hypothesis
H_0	Null hypothesis.
I_d	Diffusion Chronomal (Dimensionless Time), **dimensionless.**
k_B	Boltzmann constant **1.38×10^{-23} M.L.^{2}/Θ^2.K.**
K	Aggregation rate constant **L^3/Θ.No.**
L	Spherical particle size (radius) **L.**
L_0	Nuclei particle size **L.**
m	Number of nuclei of size L_0 that make up λ_0 **No.**
n	Fractal dimension, **dimensionless.**
N_i	Total number of particles of type i per unit volume **No./L^3.**
N_T	Total number of particles present per unit volume **No./L^3.**
r_i	Particle size (radius) of i^{th} particle **L.**
r_{ij}	Collision radius of aggregate ($= r_i + r_j$) **L.**
t	Time Θ.
$t_{1/2}$	$1/(K N_0)$ half life for aggregation Θ.
T	Absolute temperature **T.**
x	An integration variable for the range of particle sizes **L.**
$\bar{x}$	Number, length mean diameter **L.**
(x^2)	Number, surface mean diameter **L^2.**
W	Colloid stability factor, **dimensionless.**

Greek letters

β	Ratio, aggregation rate to growth rate, **dimensionless.**
η^0	Constant nuclei population at time zero and size L_0 **No./L^3.L.**
η^1	Nuclei population as a function of time and size L_0 **No./L^3.L.**
$\eta(L,t)$	Number population density **No./L^2.L.**
η_i	Population density at the i^{th} particle size **No./L^3.L.**
λ_0	Size of aggregate growth unit (radius) **L.**
μ	Viscosity **M/L.Θ.**
Φ	Ratio of nuclei density to total particle density, **dimensionless.**
τ	Characteristic time Θ.

Subscripts

i	Colliding i^{th} particle of size L.
j	Colliding j^{th} particle of size L.
k	New Aggregated particle k, formed from collision of the i^{th} and j^{th} particles.

Note: Fundamental dimensions are defined as follows:

No.	= Number of Particles.
M	= Mass.
L	= Length.
Θ	= Time.
T	= Temperature.

References

1. Demchak R, Matijevic E (1969) J Colloid Interface Sci 31:257
2. Brace R, Matijevic E (1973) J Inorg Nucl Chem 35:3691
3. Matijevic E, Scheiner P (1978) J Colloid Interface Sci 66:447
4. Ishikawa T, Matijevic E (1988) J Colloid Interface Sci 123:122
5. Gherardi P, Matijevic E (1988) Colloids and Surfaces 32:257
6. Wilhelmy RB, Matijevic E (1987) Colloids and Surfaces 22:111

7. La Mer VK, Dinger RH (1950) J Am Chem Soc 72:4847
8. Nielsen AE (1964) The Kinetics of Precipitation. Pergamon Press, New York
9. Jean JH, Ring TA (1986) Langmuir 2:251
10. Ogihara T, Mizutani N, Kato M (1989) J Am Ceram Soc 72:421
11. Dirksen JA, Ring TA, to be published by J Am Cer Soc, Fall of 1989
12. Overbeek J ThG, (1982) Adv Colloid Interface Sci 15:251
13. Petres JJ, Dezelic Gj, Tezak B (1966) Croatica Chemica ACTA, 38:277
14. Petres JJ, Dezelic Gj, Tezak B (1968) Croatica Chemica ACTA 40:213
15. Petres JJ, Dezelic Gj, Tezak B (1969) Croatica Chemica ACTA 41:183
16. Matijevic E (1989) Pure & Applied Chem 60:1479
17. Hsu WP, Ronnquist L, Matijevic E (1988) Langmuir 4:31
18. Smoluchowski M von (1917) Zeitschr Phys Chem 92:129
19. Einstein A (1906) Ann Physik 19:289
20. Randolph AD, Larson· MA (1971) Theory of Particulate Processes. Academic Press, New York, pp 41–62
21. Ives KJ (1978) The Scientific Basis of Flocculation. Skjthoff and Noordhoff, Alphen aan den Rijn, The Netherlands
22. Aoki M, Ring TA, Haggerty JS (1987) Advanced Ceramic Materials 2:3A

Received August 10, 1989
accepted December 27, 1989

Authors' address:

J. A. Dirksen
Powder Technology Laboratory (LTP)
Swiss Federal Institute of Technology
1015 Lausanne, Switzerland